REPORT DOCUMENTATION PAGE

Form Approved OMB No. 0704-0188

1. REPORT DATE *(DD-MM-YYYY)*	2. REPORT TYPE	3. DATES COVERED *(From - To)*
04-06-2003	Technical Paper	

4. TITLE AND SUBTITLE

Plasma Properties in the Plume of a Hall Thruster Cluster

5a. CONTRACT NUMBER

5b. GRANT NUMBER

5c. PROGRAM ELEMENT NUMBER

6. AUTHOR(S)

Brian Beal, Alec Gallimore (Univ. of Michigan); James Haas , William Hargus, Jr. (AFRL/PRSS)

5d. PROJECT NUMBER
1011

5e. TASK NUMBER
0011

5f. WORK UNIT NUMBER

7. PERFORMING ORGANIZATION NAME(S) AND ADDRESS(ES)

Air Force Research Laboratory (AFMC)
AFRL/PRSS
1 Ara Drive
Edwards AFB CA 93524-7013

8. PERFORMING ORGANIZATION REPORT NUMBER

AFRL-PR-ED-TP-2003-151

9. SPONSORING / MONITORING AGENCY NAME(S) AND ADDRESS(ES)

Air Force Research Laboratory (AFMC)
AFRL/PRS
5 Pollux Drive
Edwards AFB CA 93524-7048

10. SPONSOR/MONITOR'S ACRONYM(S)

11. SPONSOR/MONITOR'S NUMBER(S)
AFRL-PR-ED-TP-2003-151

12. DISTRIBUTION / AVAILABILITY STATEMENT

Approved for public release; distribution unlimited.

13. SUPPLEMENTARY NOTES

For presentation in the Journal of Propulsion and Power.

14. ABSTRACT

15. SUBJECT TERMS

16. SECURITY CLASSIFICATION OF:			17. LIMITATION OF ABSTRACT	18. NUMBER OF PAGES	19a. NAME OF RESPONSIBLE PERSON
a. REPORT	b. ABSTRACT	c. THIS PAGE			Leilani Richardson
Unclassified	**Unclassified**	**Unclassified**	A	37	19b. TELEPHONE NUMBER *(include area code)* (661) 275-5015

Plasma Properties in the Plume of a Hall Thruster Cluster

Brian Beal and Alec Gallimore

Plasmadynamics and Electric Propulsion Laboratory

University of Michigan, Ann Arbor, MI 48109

James Haas and William Hargus, Jr.

Spacecraft Propulsion Branch

Air Force Research Laboratory, Edwards AFB, CA 93524

ABSTRACT

The Hall thruster cluster is an attractive propulsion approach for spacecraft requiring very high-power electric propulsion systems. This article presents plasma density, electron temperature, and plasma potential data collected with a combination of triple Langmuir probes and floating emissive probes in the plume of a low-power, four-engine Hall thruster cluster. Simple analytical formulas are introduced that allow these quantities to be predicted downstream of a cluster based solely on the known plume properties of a single thruster. Ion energy distribution functions measured using both a parallel plate electrostatic analyzer and a retarding potential analyzer are presented. A cluster of Hall thrusters is shown to exhibit dramatically different ion energy profiles compared to a single thruster. In particular, clustering causes a significant increase in the fraction of ions at energies below the primary peak in the distribution, most likely due to an increase in elastic scattering and the effects of the unique plasma potential profiles in the cluster plume.

Nomenclature

A = Area of one electrode

B = Magnetic field strength

d = Energy analyzer plate separation distance

e = Electron charge

E = Electric field strength

k_b = Boltzmann's constant

K_{45} = Spectrometer constant for 45° energy analyzer

L = Distance between slits in energy analyzer baseplate

m_i = Ion mass

m_e = Electron mass

n_e = Electron number density

n_0 = Reference density

q_i = Ion charge

T_e = Electron temperature

u_i = Initial ion velocity

V_b= Ion beam voltage

V_{d2} = Voltage measured between triple probe electrodes 1 and 2

V_{d3} = Voltage applied between triple probe electrodes 1 and 3

V_i = Equivalent ion voltage, $m_i u_i^2/(2q_i)$

V_f = Floating potential

V_R = Energy analyzer reflector plate voltage

ϕ = Plasma potential

ϕ_T = Thermalized potential

j = Subscript denoting the contribution from an individual thruster

Introduction

Future space missions will require electric propulsion systems capable of operating at very high power levels compared to those currently in use.[1,2] One method being considered for reaching these power levels involves clustering multiple moderately-powered devices together to reach the total throughput desired. The most viable type of electric propulsion device for this class of mission is the Hall thruster due to its low specific mass, high thrust density, and high reliability.[1,2] In an effort to understand the technical issues related to operating multiple Hall thrusters in close proximity to each other, a cluster of four Busek BHT-200-X3 200-watt class devices is being studied.[3-5]

A cluster of thrusters may have a slightly lower efficiency and higher dry mass than a single, similarly powered thruster since larger engines have historically outperformed smaller thrusters. A cluster, however, has several advantages over a monolithic thruster, including improved system reliability due to the inherent redundancy of running multiple engines and the ability to throttle the system by simply turning off one or more thrusters. Throttling the system in this way allows the cluster to operate at lower power without running any of the individual thrusters at off-design conditions. This characteristic of a cluster may prove beneficial on missions where either the available power or the propulsive needs change as a function of time. For example, a high-power cluster of Hall thrusters could be used for the initial low-earth orbit to

geosynchronous orbit (LEO-GEO) transfer of a geosynchronous communications satellite. Upon reaching its final destination, one element of the cluster could then be used for north-south station keeping. A final advantage of clustering is the high degree of system scalability. In principle, once the technical issues involved with operating a cluster are fully understood, a single flight-qualified engine could support a wide range of missions requiring various power levels by simply clustering the appropriate number of thrusters. Thus, enhanced scalability and flexibility make clusters attractive for many missions.

Although using a cluster of commercially available thrusters for primary propulsion appears to be advantageous for some missions, there are several systems integration issues that must be addressed before clusters can be used in flight.[1,2] In particular, it is imperative that the interaction of the plasma plumes both among the thrusters and with the spacecraft be understood. In an effort to address this issue, the ion energy distribution downstream of a low-power Hall thruster cluster is studied using both a parallel-plate electrostatic analyzer (ESA) and a retarding potential analyzer (RPA). Additionally, the electron number density, electron temperature, and plasma potential downstream of the cluster are measured using a combination of electrostatic probes. In each case, the profiles recorded in the cluster plume are compared to those measured downstream of an individual thruster.

Experimental Apparatus

Cluster

The cluster used in this experiment is composed of four Busek BHT-200-X3 200-watt class Hall thrusters. An earlier version of this thruster is reported to operate at an anode efficiency of 42% and specific impulse of 1300 seconds while providing 12.4 mN of thrust at the nominal operating conditions.[6] Each thruster has a mean diameter of 21 mm and is operated on xenon propellant. The thrusters are arranged in a 2x2 grid with approximately 11.4 centimeters between the centerlines of adjacent thrusters. Typical operating conditions for the BHT-200 are given in Table 1.[3] Figure 1 shows the cluster during operation.

Table 1: Typical operating conditions for the BHT-200 Hall thruster.

Parameter	Value
Discharge Voltage (V)	250 ± 0.5
Discharge Current (A)	0.80 ± 0.03
Cathode Potential (V)	-8.5 ± 1.0
Electromagnet Current (A)	1.0 ± 0.03
Keeper Current (A)	0.5 ± 0.05
Keeper Voltage (V)	13 ± 1
Anode Mass Flow Rate (sccm)	8.5 ± 0.85
Cathode Mass Flow Rate (sccm)	1.0 ± 0.1

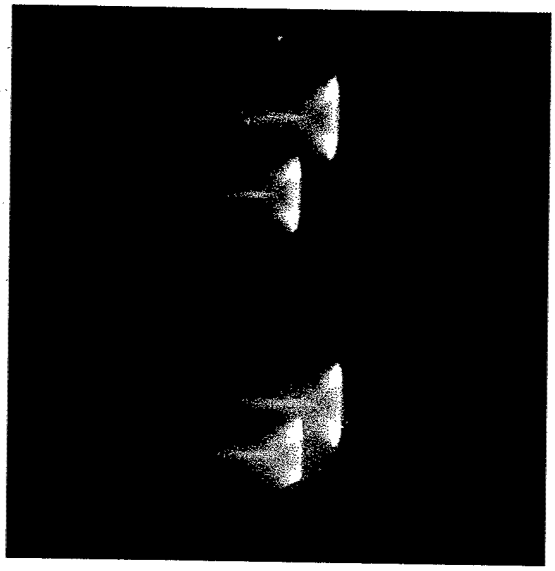

Fig. 1: A low-power cluster in operation.

Vacuum Facilities

The electron number density, electron temperature, and plasma potential measurements presented in this paper are obtained in Chamber 6 at the Air Force Research Laboratory (AFRL). Chamber 6 is a 1.5 x 2.4 meter cylindrical, stainless steel vacuum chamber that is evacuated by one dual-stage cryopump and four single-stage cryopanels. During thruster operation, the chamber pressure stabilizes at approximately 6.1×10^{-6} Torr for single thruster operation and 2.3×10^{-5} Torr for four-thruster operation. Both reported pressures are corrected for xenon.

Measurements of ion energy distributions are conducted in the Large Vacuum Test Facility (LVTF) at the University of Michigan's Plasmadynamics and Electric Propulsion Laboratory (PEPL). The LVTF is a 6x9 meter, cylindrical, stainless steel clad vacuum chamber that is evacuated by seven cryopumps, which provide a pumping speed of 500,000 liters per second on air and 240,000 liters per second on xenon for typical base pressures of approximately 2.5×10^{-7} Torr. For these experiments, only four

cryopumps were used resulting in chamber pressures of 1.1×10^{-6} and 3.6×10^{-6} Torr (corrected for xenon) during single- and four-thruster operation, respectively.

Coordinate System

The naming convention and coordinate system used throughout this experiment are shown in Fig. 2. As shown, the thrusters are labeled as TH 1-4 beginning in the upper left-hand corner and proceeding counterclockwise. The origin of the coordinate system is defined as the midpoint of the cluster in the displayed X-Y plane. The Z coordinate measures the distance downstream of the thruster exit plane. A three-dimensional positioning system is used to sweep probes through the plasma plume.

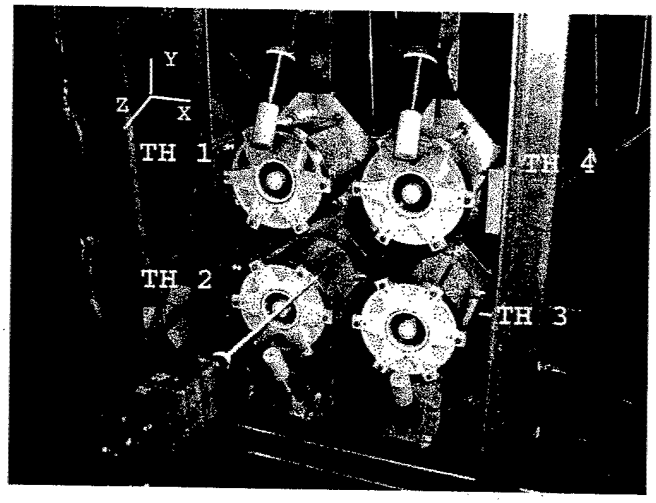

Fig. 2: Thruster naming convention and coordinate system.

Triple Probe

The triple Langmuir probe used for these experiments consists of 3 tungsten electrodes insulated from each other by an alumina rod. Each electrode is 0.5 mm (0.020") in diameter and 5.0 mm (0.20") long. The spacing between the centerlines of

adjacent electrodes is approximately 2 mm. The probe is sized to criteria that allow the standard "thin sheath" assumptions of probe theory to be applied.[7] These criteria, which are discussed elsewhere,[8] are necessary to ensure proper operation of the probe.

The symmetric triple probe, originally developed by Chen and Sekiguchi,[9] is a convenient plasma diagnostic for collecting large amounts of data due to the elimination of the voltage sweep required by other electrostatic probes. Additionally, since the probe as a whole floats, the disturbance to the ambient plasma is minimized compared to single Langmuir probes, which draw a net current from the discharge. The relations used to determine plasma parameters from the measured quantities are given in Eqns. 1 and 2. Various error analyses indicate that the uncertainty in the calculated electron temperature and number density are generally less than 30% and 60%, respectively.[9, 10] The relative uncertainty between multiple data points recorded using the same probe is believed to be significantly lower than the absolute uncertainty.

$$n_e = \left(\frac{em_i}{k_b T_e}\right)^{1/2} \frac{I \exp\left(\frac{1}{2}\right)}{Ae^{3/2}\left[\exp\left(\frac{eV_{d2}}{k_b T_e}\right) - 1\right]} \tag{1}$$

$$\frac{1-\exp\left(\frac{-eV_{d2}}{k_b T_e}\right)}{1-\exp\left(\frac{-eV_{d3}}{k_b T_e}\right)} = \frac{1}{2} \tag{2}$$

Emissive Probe

Plasma potential measurements are conducted using a floating emissive probe similar to the one described by Haas *et al.*[11] The emitting portion of the probe consists of a 0.127 mm (0.005") diameter tungsten filament loop, the ends of which are inserted into

double bore alumina tubing along with 0.508 mm (0.020") diameter molybdenum wire leads. Short lengths of tungsten wire are inserted into the alumina tube to insure contact between the emitting filament and molybdenum leads. The diameter of the emitting filament loop is approximately 3 mm. Figure 3 shows a sketch of the emissive probe.

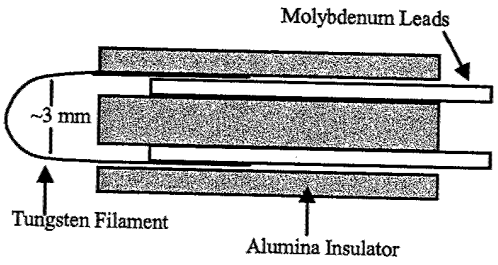

Fig. 3: The floating emissive probe.

The theory of the emissive probe is well established and results in the conclusion that a thermionically emitting filament will assume the local plasma potential when its emitted electron current is sufficient to neutralize the plasma sheath.[12] For this experiment, the current necessary to heat the probe is provided by a programmable power supply with floating outputs. At each location in the plume, the current is steadily increased and the potential with respect to ground at the negative terminal of the supply is recorded. This method allows for verification of a well-defined plateau in the voltage-current trace, which indicates plasma sheath neutralization. Considering that the voltage drop across the emitting filament never exceeds 6 V, the uncertainty in the plasma potential measurements is estimated to be ±3 V.

Electrostatic Energy Analyzer

A 45°, parallel-plate type electrostatic energy analyzer (ESA) consists of two parallel plates separated by a distance, d. One of the plates is electrically grounded while

the other is biased to a positive potential, V_R, to reflect ions admitted through a slit in the grounded baseplate. After being deflected by the applied electric field, ions of a selected initial velocity to charge ratio, u_i/q_i, pass through a second slit and are collected by a detector as illustrated in Fig. 4. Since only ions of a specific energy to charge ratio are collected, the ESA acts as a velocity per charge filter for a given ion species. For the specific case of a 45° ion injection angle, the properties of the collected ions are related to the voltage of the repelling plate by Eqn 3. Introducing the equivalent ion voltage allows the relationship to be written in the simple form of Eqn. 4. Thus, the collector current measured as a function of the applied plate voltage is proportional to the ion energy per charge distribution. Note that this result is independent of the ion mass.

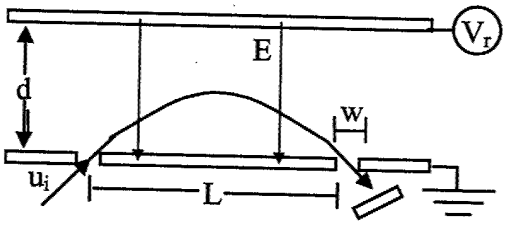

Fig. 4: Simplified schematic of a parallel plate electrostatic energy analyzer.

$$\frac{m_i u_i^2}{2q_i} = \left(\frac{L}{2d}\right) V_R \tag{3}$$

$$V_i = K_{45} V_R \tag{4}$$

The main body of the ESA consists of a cube constructed of mica dielectric and measuring approximately 300 mm (12") in each dimension. It is very similar in size to an instrument used successfully by Pollard to study a Hall thruster plume.[13] The parallel plates are constructed of 1.6 mm thick aluminum and have the following relevant

dimensions: L=152.4 mm, d=76.2 mm, and w=1.5 mm. Two field correction plates are placed between the main plates at equal intervals and biased by resistor strings to reduce the adverse effects of fringing electric fields. During data collection, V_R is swept from 0 to 600 Volts and the resulting current to the grounded collector plate is recorded using a picoammeter. Multiple ESA traces recorded at each data point demonstrate excellent repeatability, as illustrated elsewhere.[5]

Retarding Potential Analyzer

The retarding potential analyzer (RPA) diagnostic allows the collection of selectively filtered ions by applying a retarding potential across an inlet grid. For a given grid potential, only ions with energy to charge ratios greater than the grid voltage pass through the inlet and reach the collector. The magnitude of the derivative of the resulting current-voltage characteristic is then proportional to the ion energy per charge distribution. The RPA used in these experiments is based on the multi-gridded energy analyzer design of Hutchinson.[14] It is composed of three grids and is shown schematically in Fig. 5.

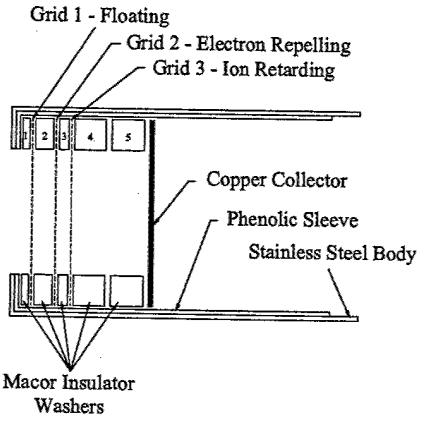

Fig. 5: The retarding potential analyzer.

The outer body of the RPA is constructed of 316 stainless steel (SS) tubing, and a phenolic sleeve placed inside the body provides electrical isolation of the grids. Each of the identical grids are cut from 0.127 mm (0.005") thick 316 SS, photochemically machined sheet with 0.279 mm (0.011") diameter openings. The grids have an open area fraction of 38% and are separated by Macor washers.

During operation, grid 1 is floated to provide a non-perturbing interface between the probe and the plasma while grid 2 is biased 30 V below ground to repel electrons. Grid 3 is swept from 0 to 600 V with respect to ground and the resulting current to the collector is measured using a picoammeter. A sample RPA current-voltage trace, a cubic spline fit to the data, and the corresponding ion energy distribution function are shown in Fig. 6. These data were taken 0.5 m downstream of the exit plane of a single thruster, 5° off centerline.

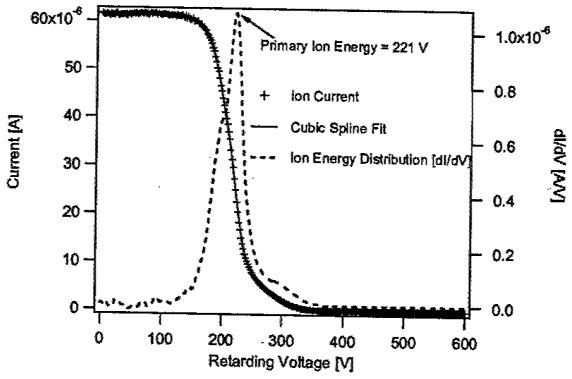

Fig. 6: Sample RPA data and resulting ion energy profile.

Gaussmeter

The magnetic field downstream of the cluster is recorded using an FW Bell model 7030 three-axis gaussmeter. All measurements are recorded without the thrusters in operation. Although recent work has shown the magnetic field profiles inside an

operating Hall thruster to deviate from the applied profiles due to fields induced by the azimuthal electron drift,[15] the difference is expected to be negligible for the low-power thrusters studied here because of the low current levels involved. The magnetic field profiles presented in this paper are, therefore, believed to be realistic representations of those that occur downstream of an operational cluster.

Results and Discussion

Magnetic Field

Figure 7 shows magnetic field data recorded in the XZ plane of thrusters 2 and 3 and in the YZ plane of thrusters 3 and 4. The differences in these plots are attributable to the different direction of magnet current flow between thrusters 2 and 4. Thrusters 2 and 3 are operated with the electromagnets in the nominal configuration while the current flow was reversed in thruster 4. Reversing the polarity of electromagnets in alternate thrusters of a cluster has been suggested as a means of canceling the disturbance torques that typically result from the slight ExB drift of the beam ions.[1,2,16] The data presented in Figs. 6 and 7 will be used to test the previously published theory that the plasma potential profiles of a cluster can be predicted from magnetic field data.[4]

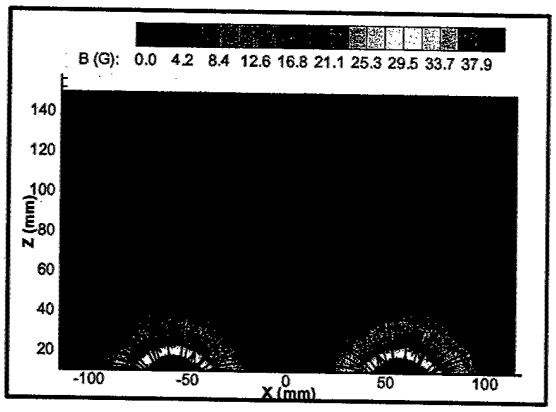

a.

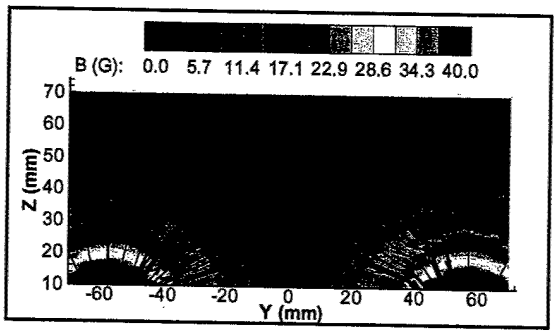

b.

Fig. 7: Magnetic field profiles downstream of a.) thrusters 2 & 3 and b.) thrusters 3 &4.

Plasma Density

A triple Langmuir probe is used to measure the plasma number density at 5 mm intervals in the cluster plume. Data are recorded in both the XZ plane of thrusters 2 and 3 and the YZ plane of thrusters 3 and 4. For both planes, data are recorded with each thruster operating alone and with two thrusters operating simultaneously. Due to the good agreement between the two data sets, only the data recorded in the YZ plane of thrusters 3 and 4 are reported here.

The plasma density profiles downstream of thrusters 3 and 4 are shown in Fig. 8. As this plot shows, the maximum number density 50 mm downstream of the cluster exit plane is roughly $1x10^{18}$ m^{-3}. This value decreases rapidly in the downstream direction and by Z=250 mm the maximum plasma density has decreased by more than an order of magnitude to about $5x10^{16}$ m^{-3}. Figure 8 shows a well-defined jet structure downstream of each individual thruster. By about 250 mm downstream the plumes have merged to the point that the density is nearly constant across the width of the cluster and resembles the profile that would be expected downstream of a large monolithic thruster.

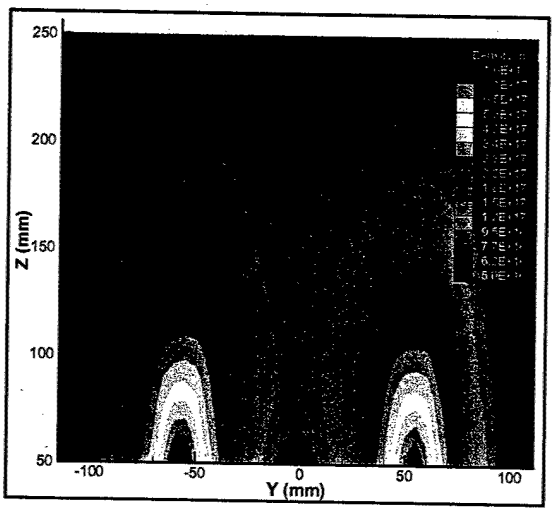

Fig. 8: Plasma density downstream of thrusters 3 and 4.

Figure 9 shows plasma density profiles at axial distances of 50, 150, and 250 mm downstream of the cluster exit plane. The unmarked lines in these plots are obtained by linear superposition of the data recorded with thruster 3 and thruster 4 running independently. The measurements of plasma density taken with both thrusters operating simultaneously agree with the calculated values to well within the margin of error of the triple probe diagnostic. This implies that the density in a cluster plume can be predicted by summing the contributions of each individual thruster, as shown in Eqn. 5.

$$n = \sum_j n_j \tag{5}$$

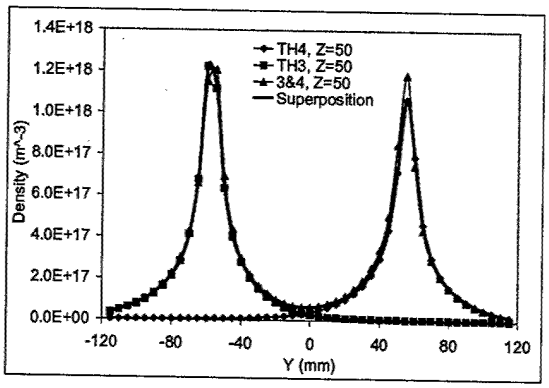

a.

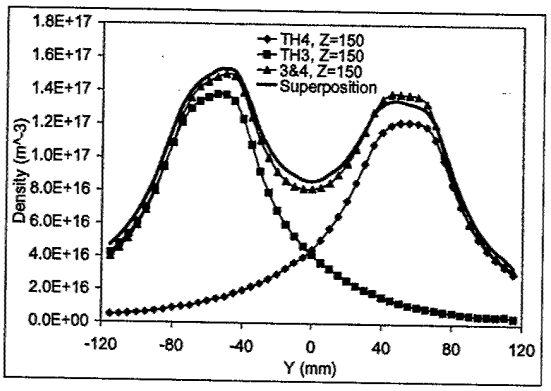

b.

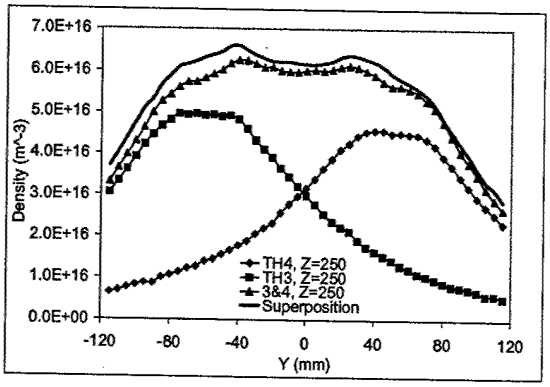

c.

Fig. 9: Plasma density a.) 50 mm, b.) 150 mm, and c.) 250 mm downstream of thrusters 3 and 4.

Electron Temperature

The electron temperature contours recorded downstream of thrusters 3 and 4 are displayed in Fig. 10. The temperature varies between roughly 3 eV at Z=50 mm along the thruster centerlines to less than 1 eV near the boundaries of the sampled region. The data show slight discrepancies in the electron temperature in the near-field of each individual thruster. Measurements recorded downstream of thrusters 2 and 3 (not shown) indicate similar differences, thus the variations are not believed to be a result of the

reversed magnetic field profiles mentioned previously. Rather, the discrepancies are probably due to tolerances in the manufacturing process or differences in the cumulative time of operation between the devices. The difference in the electron temperature in front of each thruster decreases as a function of downstream distance and by roughly Z=90 mm the difference between the two units becomes negligible.

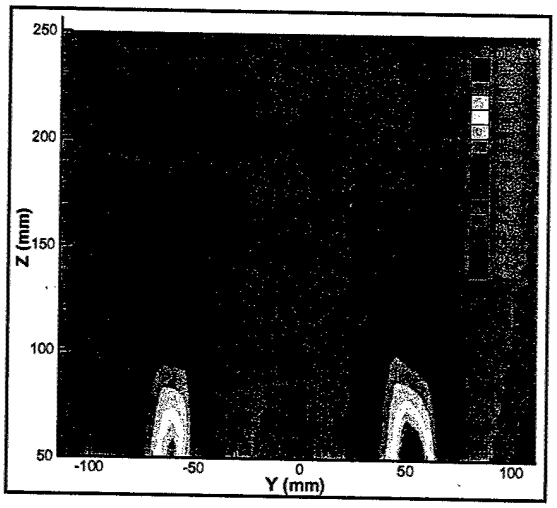

Fig. 10: Electron temperature profiles downstream of thrusters 3 and 4.

Electron temperature traces measured at axial locations of 50, 150, and 250 mm are shown in Fig. 11. The unmarked line in each plot is calculated using Eqn. 6 and represents a first attempt to predict the electron temperature in the cluster plume. The simplistic approach of calculating a density weighted average, as indicated by Eqn. 6, seems to slightly underpredict the measured temperature, particularly in the region between the thrusters. The electron temperatures measured during thruster operation are consistently higher than those recorded during single thruster operation; however the difference is generally less than 0.2 eV, which is within the uncertainty of the diagnostic.

$$\frac{k_b T_e}{e} = \frac{\sum_j n_j \frac{k_b T_{ej}}{e}}{\sum_j n_j} \tag{6}$$

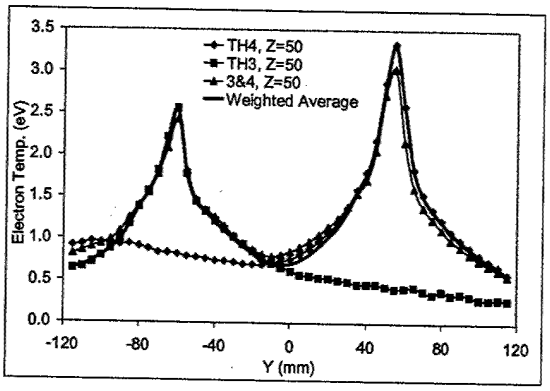

a.

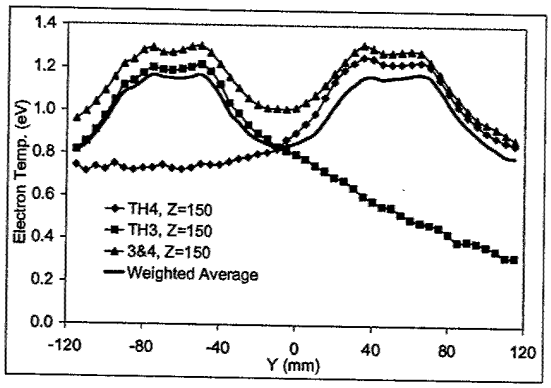

b.

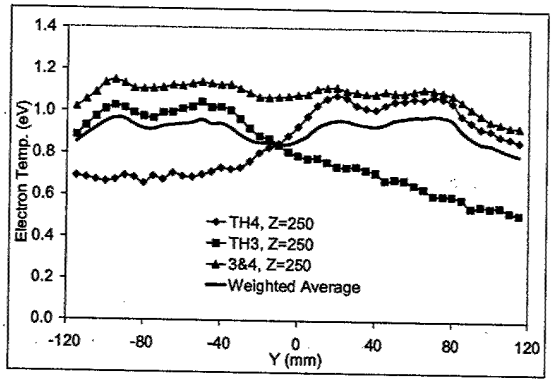

c.

Fig. 11: Electron temperature at a.) Z=50 mm, b.) Z=150 mm, c.) Z=250 mm.

Plasma Potential

An emissive probe is used to measure the plasma potential at 5 mm intervals in the cluster plume. Results obtained with thrusters 3 and 4 operating simultaneously are

shown in Fig. 12. An interesting feature shown in this plot is the unique plasma potential profile in the area between the thrusters. Between approximately Y=-30 and Y=30 mm, the plasma potential increases with downstream distance indicating that there exists a region where the electric field vector is oriented in the upstream direction. This can be seen clearly in Fig. 13, which shows the plasma potential profiles at various axial locations. The reversed electric field could potentially cause ions produced in the area between the thrusters to be accelerated upstream toward the spacecraft on which the thrusters are mounted. Although this could hypothetically result in an increased erosion rate in some areas due to increased ion impingement, the effect is expected to be negligible since the impinging ions are unlikely to experience accelerating potentials greater than a few volts in the reverse direction.

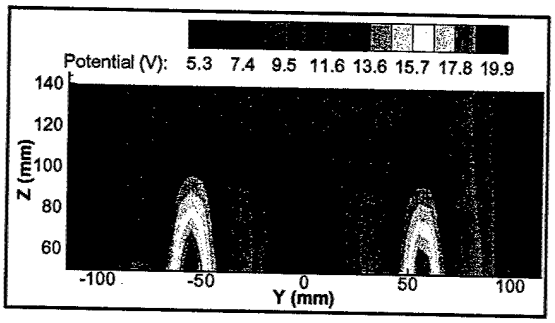

Fig. 12: Plasma potential downstream of thrusters 3 and 4.

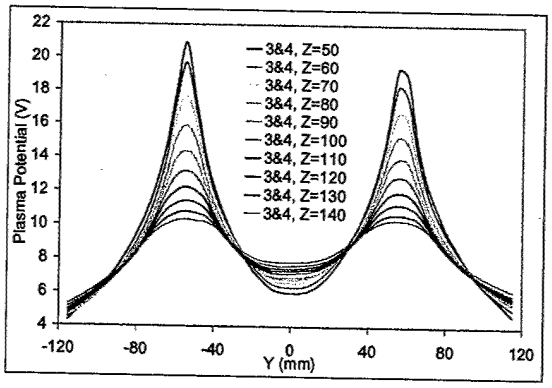

Fig. 13: Plasma potential profiles downstream of two operating Hall thrusters.

It has been suggested that the plasma potential profiles downstream of a cluster could be predicted by simply integrating the magnetic field data.[4] This is contradicted by the measurements presented in Fig. 14, which shows the plasma potential downstream of thrusters 3 and 4 at axial distances of 60, 100, and 140 mm. Clearly, integration along the magnetic field lines depicted in Fig. 7b does not result in the observed potential profiles.

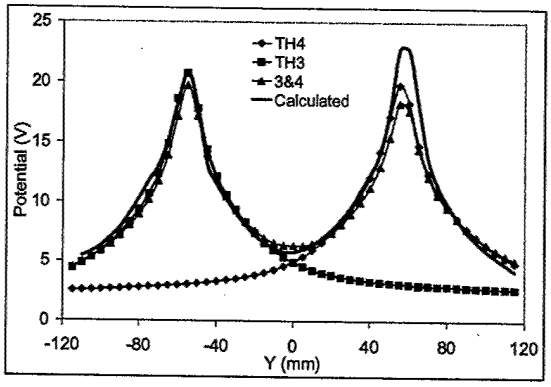

a.

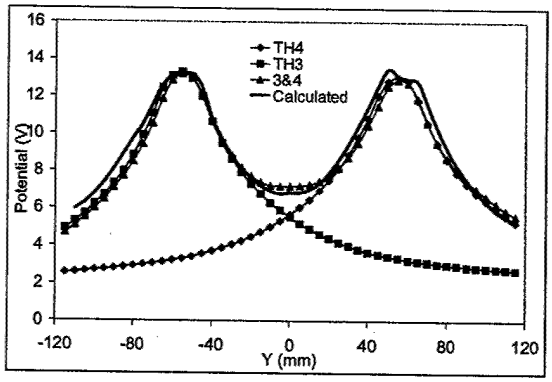

b.

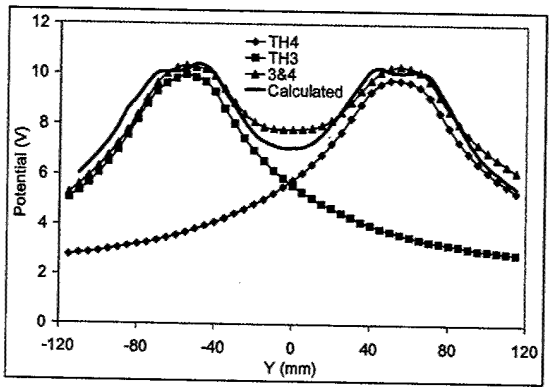

c.

Fig. 14: Plasma potential profiles at a.) Z=60 mm, b.) Z=100 mm, and c.) Z=140 mm.

A more conventional method for relating the magnetic field architecture to the plasma potential involves consideration of electron dynamics in a plasma. Along a magnetic field line, the motion of electrons is governed purely by electrostatic forces and can be described by the well known Boltzmann relation.[17] This leads naturally to the definition of a thermalized potential, ϕ_T, which is given by Eqn. 7 and conserved along a line of force.[18] In the derivation of Eqn. 7, the electron temperature has been assumed constant along lines of force.

$$\phi_T \equiv \phi - \frac{k_B T_e}{e} \ln\left(\frac{n}{n_0}\right) \tag{7}$$

The concept of thermalized potential is useful in the design of Hall thrusters since it shows that the magnetic field lines can be approximated as equipotential lines in situations where the electron temperature is negligible compared to the plasma potential. In other words, the thermalized potential is a useful tool for predicting plasma potential in situations where electrons are tightly bound to the magnetic field lines. This method,

however, is less useful in the thruster plume since the correction term due to thermal effects and density gradients can be as large as the plasma potential.

Comparing the plasma potential data of Fig. 12 to the magnetic field profiles shown in Fig. 7b, it is clear that the lines of force do not correspond to equipotential contours. This is not surprising, since the magnetic field strength is generally less than 10 G and the electrons are only weakly magnetized throughout the areas where the plasma potential is presented. In this situation, thermal effects and density gradients are dominant over the effects of the magnetic field, and the plasma potential is described by the Boltzmann relation given by Eqn. 8.[19] The profiles calculated using Eqn. 8 are shown in Fig. 14 and generally agree to within one volt of the measured values, except in the most upstream locations of the sampled region. In utilizing Eqn. 8, the reference density (n_0=7x10^{17} m^{-3} in this case) is chosen so as to make the plasma potential calculated along the centerline of thruster 3 at Z=100 mm match the measured value. While the choice to match the value at 100 mm is arbitrary, a similar approach is expected to be valid in most practical cluster configurations since the data presented here shows the plasma potential directly downstream of one thruster to be largely unaffected by the surrounding devices. Implementation of Eqn. 8 along with Eqns. 5 and 6 thus allows the most basic plasma properties downstream of a cluster of identical Hall thrusters to be predicted based solely on measurements or simulations of a single unit. Results obtained in this way appear to be accurate to within the margin of error of typical plasma diagnostics.

$$\phi = \frac{k_B T_e}{e} \ln\left(\frac{n}{n_0}\right) \tag{8}$$

Single Thruster Ion Energy Profiles

As an initial test of the energy analysis diagnostics, energy distributions measured with the RPA are compared to those measured with the ESA for a single thruster. Figure 15 shows the measured distribution function for a single thruster at 0°, 15°, and 30° off centerline for each instrument. Notice the relatively good agreement between the two devices. For each of the three angular locations, the voltage at which the peak in the distribution function occurs agrees to within 8 volts. For example, on the thruster centerline the primary peak was measured at 220 volts by the RPA and at 228 volts by the ESA.

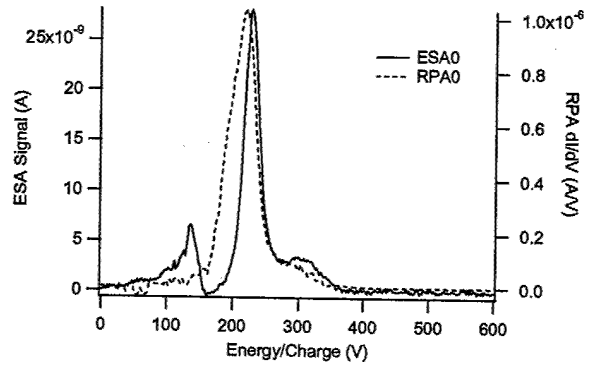

a.

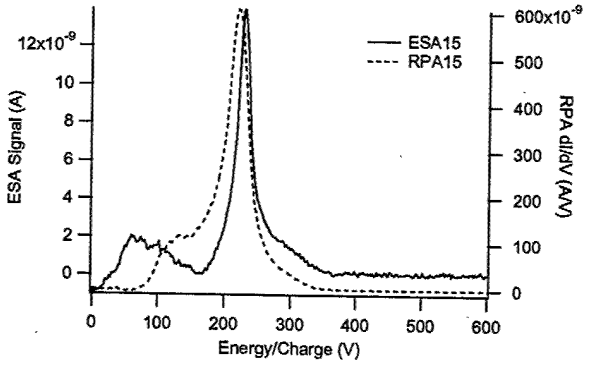

b.

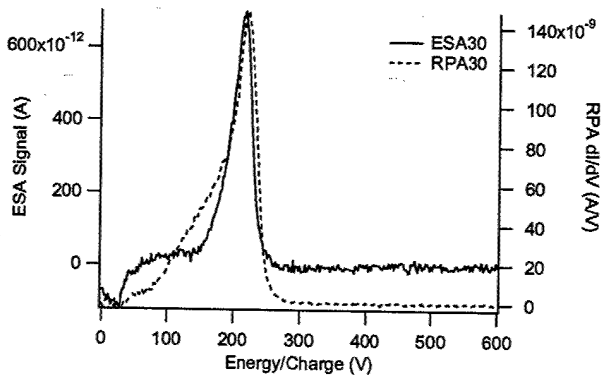

c.

Fig. 15: Comparison of ESA and RPA diagnostics 0.5 m downstream of a single Hall thrusters at angles of a.) 0, b.) 15, and c.) 30 degrees off centerline.

The most noticeable difference between the diagnostics demonstrated by Fig. 15 is the appearance of secondary peaks at voltages above and below the primary ion voltage, which are more pronounced in the ESA traces. Additionally, the primary peak in the distribution is consistently wider when measured with the RPA as opposed to the ESA. The shape of the distribution function is likely to be more accurate in the ESA traces since those data are not subject to the effects of numerical differentiation. The location of the primary peak in the distribution, however, is likely to be more accurately depicted by the RPA because slight misalignment of the grid components would not be expected to alter the performance of this device. Slight misalignment or improper spacing of the plates in the ESA, on the other hand, could cause a shift of several volts in the measured distributions.

Figure 16 summarizes the ion energy distributions recorded by the ESA, while Fig. 17 depicts similar data recorded by the RPA. All data are recorded 0.5 meters downstream of the thruster along a radial arc. Although traces have been recorded for

both positive and negative angles off centerline, only data for the positive angles are reported here due to the high degree of symmetry exhibited by the plume. The ESA traces show the peak ion energy to charge ratio to occur at approximately 228 volts for most of the angular spectrum, while the RPA shows the peak at 220 volts. The secondary structure occurring at energy to charge ratios below 150 volts can be attributed to elastically scattered primary ions.[13, 19] The high-energy population shown at voltages in excess of the discharge voltage, particularly at low angles off centerline, is likely due to beam ions that have undergone charge decreasing collisions.[13, 20] Data are not shown for the ESA at angles greater than 60° due to the prohibitively small signal to noise ratio in this regime. RPA data, however, show the plume to be composed primarily of low-energy charge exchange products at angles greater than 70°.

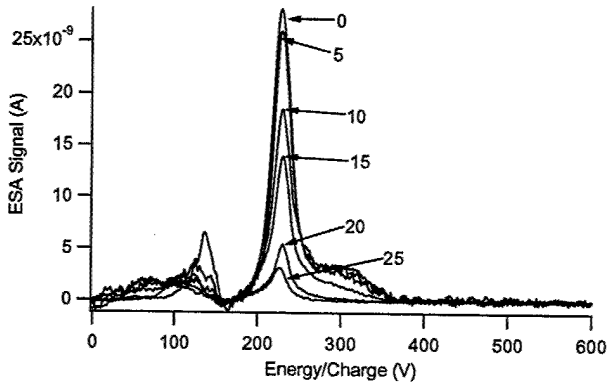

a.

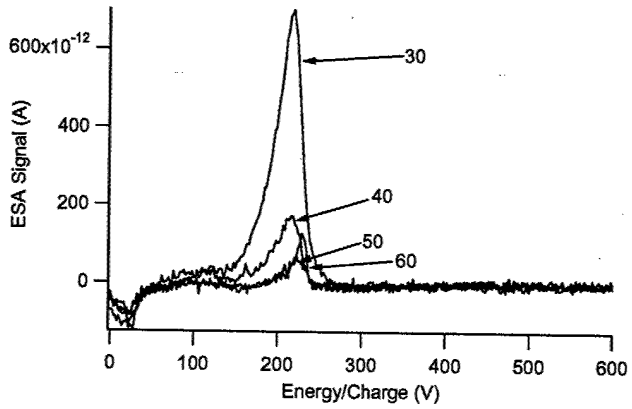

b.

Fig. 16: Energy profiles measured with the ESA in the plume of a single thruster at angles of a.) 0-25° and b.) 30-60°.

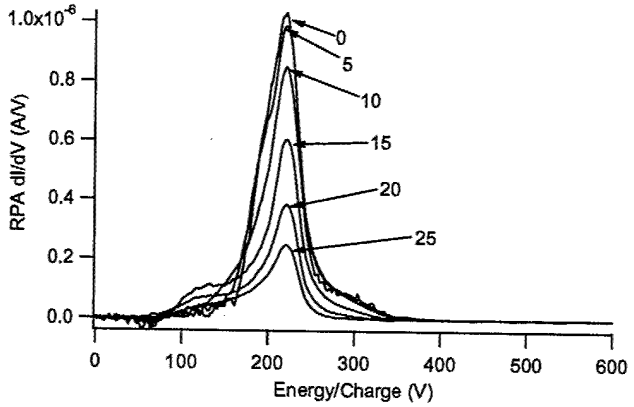

a.

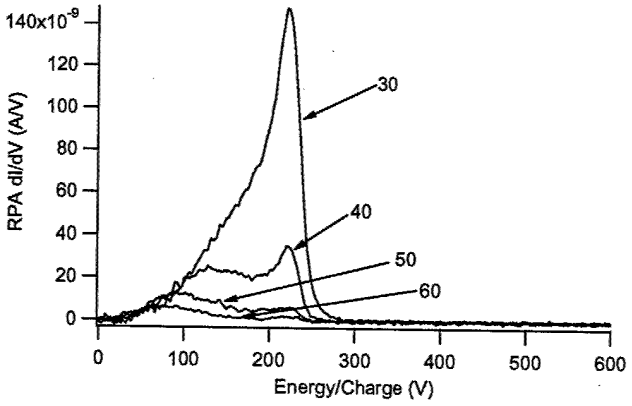

b.

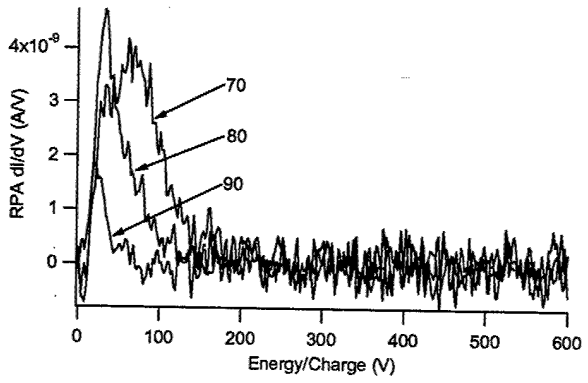

c.

Fig. 17: Single thruster RPA data at angles of a.) 0-25, b.) 30-60, c.) 70-90 degrees off centerline.

Cluster Ion Energy Profiles

Unlike the data recorded for the single thruster case, the measurements obtained with the ESA and RPA aligned to the center of the cluster show marked differences between the two diagnostics. These differences are believed to be caused primarily by the different acceptance angles of the RPA and ESA. The ESA entrance slit provides an ion acceptance angle of approximately 4° in one direction and 0.5° in the other direction, while the cylindrical RPA has an acceptance cone half angle of approximately 25°. This discrepancy is not important for the case of a single thruster because both diagnostics are able to image the entire width of the thruster at a downstream distance of 0.5 m. At this distance, the ESA images a cross section only about 70 mm wide. In the cluster configuration, this results in the ESA imaging the space between the thrusters rather than the thrusters themselves. The RPA, on the other hand, has a sufficiently wide viewing angle to accept ions originating from any of the four thrusters.

Figure 18 summarizes the cluster data collected with the parallel plate energy analyzer. At angular positions less than 10° with respect to centerline, the peak in the distribution occurs at energy to charge ratios near the 250 volt discharge voltage. Between 10° and 20° the peak shifts down to approximately 134 volts, which is near the voltage of the elastically scattered ions measured in the plume of a single thruster. The 134 volt peak can be observed out to 80° off the cluster axis before the signal is lost between 80° and 90°. It should be noted that the signal level recorded by the ESA in this configuration is approximately a factor of 25 lower than that measured for a single thruster due to the limited viewing angle.

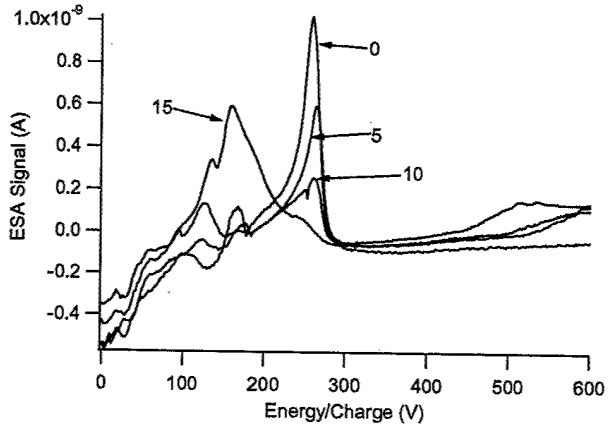

a.

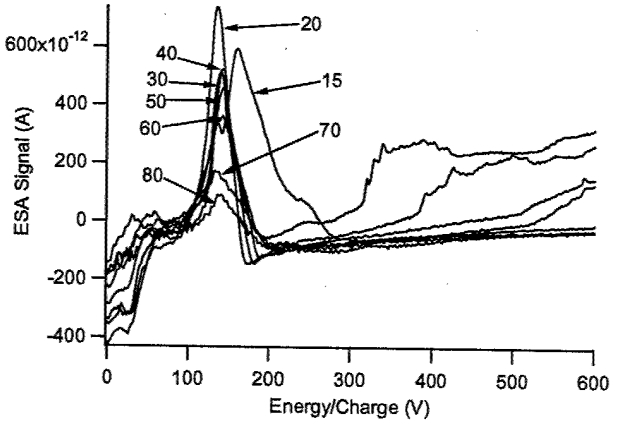

b.

Fig. 18: Ion energy profiles downstream of the cluster at angles of a.) 0-15 and b.) 15-80 degrees off centerline.

The RPA data presented in Fig. 19 show several unusual characteristics, particularly along the cluster centerline where the spectrum shows three distinct, repeatable peaks at 224, 116, and 74 volts. As explained by Gallimore, the peaks at 116 and 74 volts could be caused by ions exiting the thruster at a beam kinetic energy, V_b, of 224 volts before undergoing charge exchange (CEX) collisions that result in populations with energy to charge ratios of approximately $V_b/2$ and $V_b/3$, respectively.[20] Just 5° off centerline, however, the spectrum changes to a double peaked structure with equally abundant populations occurring at 122 and 222 volts. As the angle off centerline is increased, the two peaks merge together to form a single peak near 206 volts with a low energy tail as shown in Fig. 19b. Charge exchange collisions tend to generate signatures in the energy per charge spectra at discrete multiples of the main peak in the distribution.[20] The fact that the ratio between the observed peak voltages changes as a function of angle seems to indicate that, if the multi-peak structure is due to collisions, the dominant interactions are likely elastic rather than CEX. The existence of elastic scattering peaks at voltages below the main peak is consistent with numerical simulations that take into account recently calculated cross sections for collisions between xenon ions and neutrals.[19] The shift of the low energy population to higher voltage with increasing angle seen in Fig. 19a, however, is opposite to previously observed trends.[13] This suggests that a physical mechanism other than collisions may contribute to the low-

energy structure. At angles greater than 50° with respect to the thrust axis, the spectra are dominated by a low-energy population that shifts to lower voltage with increasing angles.

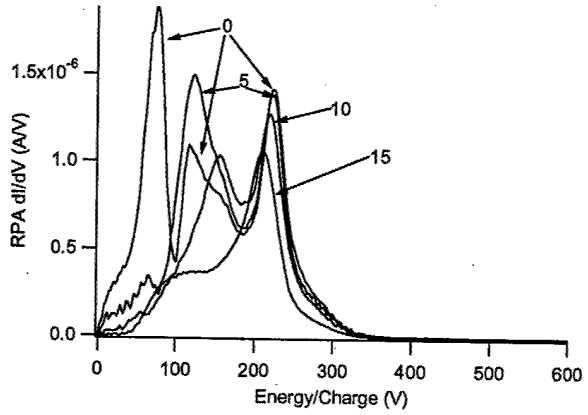

a.

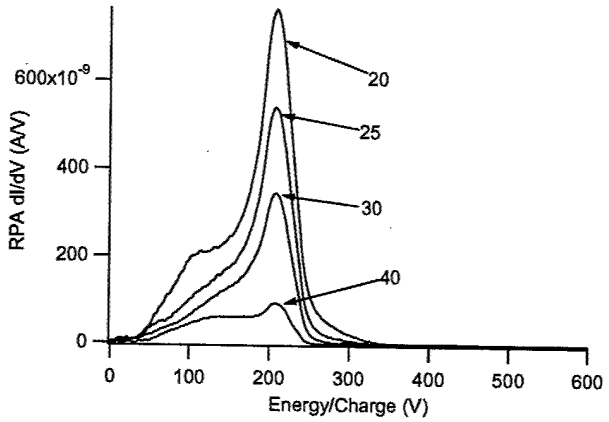

b.

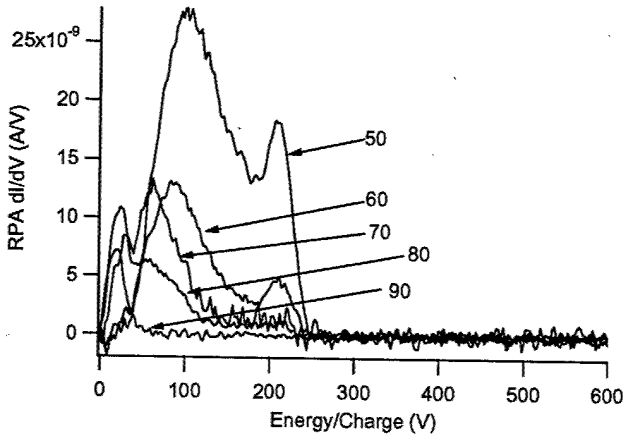

c.

Fig. 19: RPA data at a.) low, b.) medium, and c.) high angles off the cluster centerline.

In addition to collisions, a possible contributing factor to the low-energy structure involves ion focusing as a result of clustering. As shown in Figs. 12-14, the plasma potential profile downstream of a cluster is fundamentally different than the profile in the plume of a single thruster. When ions exit a single Hall thruster, they experience a continuous decline in plasma potential regardless of the direction in which they exit the thruster. In other words, the electric field vector is everywhere directed away from the device. When multiple thrusters are operated together, however, a minimum in the plasma potential occurs in the region between the thrusters. This results in a situation where an ion directed toward the center of the cluster can be deflected downstream by the plasma potential "hill" created by adjacent thrusters. This situation is sketched in Fig. 20 below, in which the dashed lines represent contours of constant plasma potential and the heavy arrows represent the paths of sample ions. The phenomenon illustrated in Fig. 20 may lead to ion focusing in which ions initially directed toward the cluster center are deflected to lower angles with respect to the cluster centerline. This effect may be responsible for the slightly reduced beam divergence reported by Hargus and Reed for two operating thrusters compared to that predicted by linear superposition of the ion flux from individual thrusters.[4]

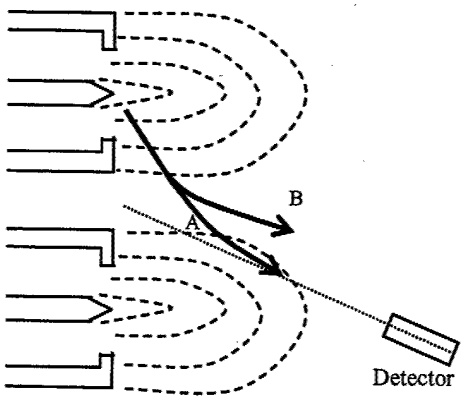

Fig. 20: Ion focusing mechanism due to clustering.

The mechanism of ion focusing presented here requires additional analysis before its effects on the plasma plume can be evaluated quantitatively. However, one can gain insight into several aspects of the energy spectrum by resorting to a simple phenomenological discussion. Consider two ions, A and B, exiting a thruster and traveling in an identical direction toward the center of the cluster, but with different initial kinetic energies. In this situation, the slower moving ion, B, would be deflected by a given potential rise to a greater extent than its high-energy counterpart, ion A, as depicted in Fig. 20. Considering this, a detector swept through the plume would detect ion A at a higher angle off centerline, while ion B with its lower energy would be deflected further downstream and detected at a relatively low angle. This phenomenon may account for the secondary structure shown in Fig. 19a, in which the low energy population shifts to higher voltages with increasing angle off centerline. This feature is only observable during cluster operation and is most pronounced at low angles.

In addition to the cluster configuration discussed above, data have also been obtained with four thrusters in operation, but with the ESA and RPA aligned to the centerline of TH 3 rather than the centerline of the cluster. These data are presented in detail elsewhere[5] and are qualitatively similar to the results discussed above. The most notable features observed in this "offset cluster" configuration are the tendency of the primary peak in the distribution to shift to lower voltages with increasing angle off centerline and the predominance of structures at energies well below the discharge voltage at angles greater than 40°. Although the secondary structure is visible in the single thruster data, its magnitude is much larger during cluster operation, which seems to indicate a dramatic increase in ion scattering due to multi-thruster operation.

Conclusions

A combination of triple Langmuir probes and floating emissive probes is used to characterize the electron number density, electron temperature, and plasma potential in the plume of a low-power Hall thruster cluster. The results show that properties in the cluster plume can be predicted using simple analytical relations and knowledge of a single thruster plume. In particular, the plasma density can be predicted by simple linear superposition while the electron temperature is estimated to be a weighted average of that due to the plumes of individual thrusters. Having obtained predictions of electron number density and electron temperature, these results are then used to estimate the resulting plasma potential via the Boltzmann relation.

Ion energy spectra are obtained using both a parallel plate electrostatic analyzer and a retarding potential analyzer at locations 0.5 meters downstream of the thruster

cluster. Compared to results obtained in the plume of a single thruster, these data indicate a profound increase in the fraction of low-energy ions measured at voltages below the primary peak in the distribution. This feature is believed to be due to an increase in elastic scattering of beam ions as well as the unique plasma potential profiles downstream of a cluster. Ion focusing as a result of the plasma potential distribution is hypothesized to be responsible for the response of low-energy structures reported here, as well as effects observed in recently published ion flux data.

Acknowledgements

The authors wish to thank Dr. Mitat Birkan of the Air Force Office of Scientific Research and Dr. David Campbell of ERC, Inc. for sponsoring this research. The authors also wish to thank Mr. Terry Larrow of the University of Michigan for his excellent work in fabricating the energy analyzer. This work was performed under the auspices of AFOSR Grant F49620-02-1-0051 and AFRL-ERC Grant RPO20870.

References

1. Spores, R. A., Spanjers, G. G., Birkan, M., Lawrence, T.J., "Overview of the USAF Electric Propulsion Program," *Proceedings of the 37th AIAA Joint Propulsion Conference*, AIAA Paper No. 2001-3225, AIAA, Washington, DC, 2001.

2. Spanjers, G. G., Birkan, M. and Lawrence, T.J., "The USAF Electric Propulsion Research Program," *Proceedings of the 36th AIAA Joint Propulsion Conference*, AIAA Paper No. 2000-3146, AIAA, Washington, DC, 2000.

3. Beal, B. E., Gallimore, A. D., and Hargus, W. A., "Preliminary Plume Characterization of a Low-Power Hall Thruster Cluster," *Proceedings of the 38th AIAA Joint Propulsion Conference*, AIAA Paper No. 2002-4251, AIAA, Washington, DC, 2002.

4. Hargus, W. A., and Reed, G., "The Air Force Clustered Hall Thruster Program," *Proceedings of the 38th AIAA Joint Propulsion Conference*, AIAA Paper No. 2002-3678, AIAA, Washington, DC, 2002.

5. Beal, B. E., and Gallimore, A. D., "Energy Analysis of a Hall Thruster Cluster," *Proceedings of the 2003 International Electric Propulsion Conference*, IEPC Paper No. 2003-0035, Electric Rocket Propulsion Society, Santa Fe, NM, 2001.

6. Hruby, V., Monheiser, J., Pote, B., Rostler, P., Kolencik, J., and Freeman, C., "Development of Low-Power Hall Thrusters," *Proceedings of the 1999 AIAA Plasmadynamics and Lasers Conference*, AIAA Paper No. 99-3534, AIAA, Washington, DC, 1999.

7. Schott, L., "Electrical Probes," *Plasma Diagnostics*, edited by W. Lochte-Holtgreven, AIP Press, Woodbury, NY, 1995, pp. 668-731.

8. Beal, B. E., Gallimore, A. D., and Hargus, W. A., "Evidence of Collisionless Shocks in a Hall Thruster Plume," submitted to *Physics of Plasmas*.

9. Chen, S. and Sekiguchi, T., "Instantaneous Direct-Display System of Plasma Parameters by Means of Triple Probe," *Journal of Applied Physics*, Vol. 36, No. 8, 1965, pp. 2363-2375.

10. Tilley, D. L., Gallimore, A. D., Kelly, A. J., and Jahn, R. G., "The Adverse Effect of Ion Drift Velocity Perpendicular to a Cylindrical Triple Probe," *Review of Scientific Instruments (AIP)*, Vol. 65, No. 3 March 1994, 678-681.

11. Haas, J. M., and Gallimore, A. D., "Internal Plasma Potential Profiles in a Laboratory Model Hall Thruster," *Physics of Plasmas*, Vol. 8, No. 2, 2001, pp. 652-660.

12. Kemp, R. F. and Sellen Jr., J. M., "Plasma Potential Measurements by Electron Emissive Probes," *Review of Scientific Instruments*, Vol. 37, No. 4, 1966, pp. 455-461.

13. Pollard, J. E., Diamant, K. D., Khayms, V., Werthman, L., King, D. Q., and de Grys, K. H., "Ion Flux, Energy, and Charge-State Measurements for the BPT-4000 Hall Thruster," *Proceedings of the 37th AIAA Joint Propulsion Conference,* AIAA Paper No. 2001-3351, AIAA, Washington, DC, 2001.

14. Hutchinson, I.H., Principles of Plasma Diagnostics, Cambridge University Press, New York, NY, 2002, pp. 94-99.

15. Peterson, P.Y., Gallimore, A. D., Haas, J. M., "An Experimental Investigation of the Internal Magnetic Field Topography of an Operating Hall Thruster," *Physics of Plasmas*, Vol. 9, No. 10, 2002, pp. 4354-4362.

16. Manzella, D.H., "Stationary Plasma Thruster Ion Velocity Distribution," *Proceedings of the 30th AIAA Joint Propulsion Conference*, AIAA Paper No. 94-3141, AIAA, Washington, DC, 1994.

17. Keidar M. and Boyd, I.D., "Effect of a Magnetic Field on the Plasma Plume from Hall Thrusters," *Journal of Applied Physics*, Vol. 86, No. 9, 1999, pp. 4786-4791.

18. Morozov, A. I., Esipchuck, Y. V., Tilinin, G. N., Trofimov, A. V., Sharov, Y. A., Shchepkin, G. Y., "Plasma Accelerator with Closed Electron Drift and Extended Acceleration Zone," *Soviet Physics – Technical Physics*, Vol. 17, No. 1, 1972, pp. 38-45.

19. Katz, I., *et al.*, "A Hall Effect Thruster Plume Model Including Large-Angle Elastic Scattering," AIAA-2001-3355, 37th Joint Propulsion Conference & Exhibit, Salt Lake City, UT, 2001.

20. Gallimore, A. D., "Near- and Far-Field Characterization of Hall Thruster Plumes" *Journal of Spacecraft and Rockets (AIAA)*, Vol. 38, No. 3, May-June, 2001, 441-453.